Journal of Alloys and Compounds 509 (2011) 9809–9815

Contents lists available at ScienceDirect

Journal of Alloys and Compounds

journal homepage: www.elsevier.com/locate/jallcom

Comparative study of microwave and conventional methods for the preparation and optical properties of novel MgO-micro and nano-structures

N. Clament Sagaya Selvam [a], R. Thinesh Kumar [a], L. John Kennedy [b], J. Judith Vijaya [a,*]

[a] Catalysis and Nanomaterials Research Laboratory, Department of Chemistry, Loyola College, Chennai 600034, India
[b] Materials Division, School of Advanced Sciences, VIT University, Chennai Campus, Chennai 600048, India

ARTICLE INFO

Article history:
Received 12 May 2011
Received in revised form 2 August 2011
Accepted 6 August 2011
Available online 12 August 2011

Keywords:
Microwave assisted synthesis
X-ray diffraction
Electron microscopy
Optical properties

ABSTRACT

Magnesium oxide (MgO) was synthesised by a simple microwave-assisted combustion route without using any template, catalyst or surfactant. For the purpose of comparison, it was also prepared using conventional method. The as-synthesized MgO was characterized by powder X-ray diffraction (XRD), Fourier Transform infrared spectra (FT-IR), high resolution scanning electron microscopy (HR-SEM), transmission electron microscopy (TEM), Energy Dispersive X-ray analysis (EDX), diffuse reflectance spectroscopy (DRS) and Photoluminescence (PL) spectroscopy. The XRD results confirmed the formation of cubic phase MgO. FT-IR was used to investigate the adsorption of water and CO_2 on MgO surface and confirm the formation of Mg-O phase. The formation of MgO micro cubes structures was confirmed by HR-SEM. The formation of MgO nanosheets was confirmed by HR-SEM and TEM and their possible formation mechanisms were also proposed. The optical absorption and photoluminescence emissions were determined by DRS and PL spectra respectively. An attempt has been made to compare the lattice parameter and the PL intensity.

1. Introduction

Systematically manipulating the morphology and architecture of nano and micro structures has created great interest because of their obvious influence on material properties and the potential application in designing new devices with unique properties. With the size of crystallites decreasing, the energy band of semiconductor nanocrystallites evolves from sequential to discrete energy levels. This causes semiconductor nanocrystallites to display optical, electronic and structural properties that are different from those of the bulk phase. Magnesium oxide has been used as solid base catalyst for aldol addition of acetone [1], as catalyst for isomerization of butane [2] and as support for Ru and Au for isotopic exchange reaction of oxygen [3]. Synthesis of magnesium oxide nanostructures has been given much attention due to its applications in catalysis and toxic waste remediation, or as an additive in refractory, paint and superconductor products [4–6]. The morphology and properties of MgO differs and depends largely on the synthesis route and processing conditions [7]. However, the useful properties of MgO are further enhanced when used as nano-size powder with novel nano structures. Many different synthetic routes provide nanoscale MgO including sol–gel [8], hydrothermal/solvothermal [9,10], laser vaporization [11], chemical gas phase deposition [12], aqueous wet chemical method [13], surfactant methods [14], polyol-mediated thermolysis process [15]. In the above mentioned methods, limitations such as requirement of sophisticated equipments, many processing steps, more time, template, surfactant, and energy dissipation in the preparation of MgO nanostructures were observed. Microwave-assisted synthesis of materials has recently gained importance over the conventional method [16]. However the mechanism by which matter absorbs microwave energy is called dielectric heating. In this context, an important property is the mobility of the dipoles and the ability to orient them according to the direction of the electric field. This field energy is transferred to the medium and electrical energy is converted into kinetic or thermal energy. Molecular friction is often cited as a model for this behaviour. The fast changing electric field of the microwave radiation leads to a rotation of the molecules. Due to this process, "internal friction" takes place in the polar medium, which leads to a direct and almost even and rapid heating of the reaction mixture [17,18].

This results in the formation of nanoparticles, early phase formation and different morphologies within a few minutes [19,20]. However, the conventional heating systems heat the material from outer surface to the interior. This result in steep thermal gradients and the formation of bulk phase which requires high temperature and more time [21]. As a result investigations in to different scale structures and respective morphologies of MgO using simple

* Corresponding author. Tel.: +91 44 28178200; fax: +91 44 28175566.
E-mail address: jjvijayaloyola@yahoo.co.in (J.J. Vijaya).

0925-8388/$ – see front matter © 2011 Elsevier B.V. All rights reserved.
doi:10.1016/j.jallcom.2011.08.032

methods are still warranted. MgO nanoparticles have been prepared by microwave-assisted synthesis using magnesium acetate [17] and MgO nano-powders were synthesised using microwave plasma torch [22]. Thus, the novel precursors and synthetic routes will be more useful, which will then open a new way for preparing nanomaterials to control shape, crystallinity, and size distribution [23]. Hence in the present study, an attempt has been made to synthesize MgO from magnesium nitrate and urea as precursors by simple microwave-assisted combustion route using a domestic microwave oven. For the purpose of comparison, MgO was also prepared by conventional combustion route. In the microwave-assisted combustion route, the whole process takes only a few minutes to produce MgO. In our experiments, rapid combustion and crystallization using urea as fuel could generate various structural defects. It is therefore interesting to examine defect energy levels and surface states of MgO, and study their modification. Hence, the optical properties of MgO have been investigated in detail to study the effect of microwave-assisted combustion synthesis in comparison with conventional combustion route in the preparation of MgO.

2. Experimental

2.1. Preparation of magnesium oxide by simple microwave assisted combustion method and conventional combustion method

All the reagents were analytical grade obtained from Merck, India and were used as received without further purification. Stoichiometric amounts of magnesium nitrate (0.61 g) and urea (0.60 g) were dissolved separately in 10 ml of deionized water and poured into a silica crucible and stirred for 15 min to obtain clear solution. This was placed in a domestic microwave-oven (2.45 GHz, 750 W) for 10 min. Initially, the solution boiled and underwent dehydration followed by decomposition with the evolution of gases. When the solution reached the point of spontaneous combustion, it vaporized the solution and instantly became a solid. The obtained solid was washed well with alcohol and dried in an oven at 70 °C for 2 h. Urea, which served as the fuel was oxidized by nitrate to form MgO. This was labeled as sample A. In a separate experiment, the same reaction mixture was taken in the crucible and treated in a furnace at 500 °C for 2 h at a heating rate of 5 °C/min, and cooled at the same rate. The obtained powder was washed well with alcohol and dried in an oven at 70 °C for 2 h, which was labeled as sample B. The slow heating rate (5 °C/min) allows longer time for atomic diffusion, which is an important sintering factor. This means more atoms move to points of contact between powder particles, which results in better sintering [24]. However, the low heating rate means that the materials are exposed to heat for longer time and thus their grains have a tendency to grow.

2.2. Characterization of MgO

The structural characterization of MgO was performed using a Philips X'pert X-ray diffractometer with CuKα radiation at λ = 1.540 Å. The surface functional groups were analyzed by Perkin Elmer FT-IR spectrometer. Morphological studies and energy dispersive X-ray analysis of MgO have been performed with a Jeol JSM6360 high resolution scanning electron microscope. The transmission electron micrographs were carried out by Philips - TEM (CM20). The diffuse reflectance UV–visible spectra of MgO was recorded using Cary100 UV–visible spectrophotometer to estimate their energy band gap. The optical properties were recorded using Varian Cary Eclipse Fluorescence Spectrophotometer. The N_2 adsorption–desorption isotherms of the samples were measured using an automatic adsorption instrument (Quantachrome Quadrawin gas sorption analyzer) for the determination of surface area and total pore volumes.

3. Results and discussion

3.1. X-ray diffraction analysis

The structural phase of the MgO was determined by X-ray diffraction pattern. The XRD patterns were recorded twice on two batches of samples for reproducible results. As shown in Fig. 1(c, d), the observed diffraction peaks at $2\theta = 42.90^\circ$, 62.30°, 78.61°, 74.60°, and 36.70° are associated with [2 0 0], [2 2 0], [2 2 2], [3 1 1], and [1 1 1] plane, respectively. These planes are then associated with the d-spacing values of 2.10, 1.48, 1.21, 1.26, and 2.43 Å, respectively, which can be readily assigned to a cubic phase of MgO (Periclase, JCPDS No. 45-0946). Further observation revealed that the sample A (spectrum c) and sample B (spectrum d) have sharp peaks, indicating good crystallinity, but the diffraction peaks for sample A are slightly broadened because of the small crystallite size. This implies that MgO is prepared in a short time of 10 min by means of a domestic microwave oven operated at 2.45 GHz and 750 W, without any post-annealing. Furthermore, no characteristic peaks from other crystalline impurities were detected by XRD, suggesting the high purity of the MgO. For the purpose of comparison, we have recorded XRD pattern for commercial $Mg(OH)_2$ and MgO bulk, which is shown in Fig. 1(a, b).

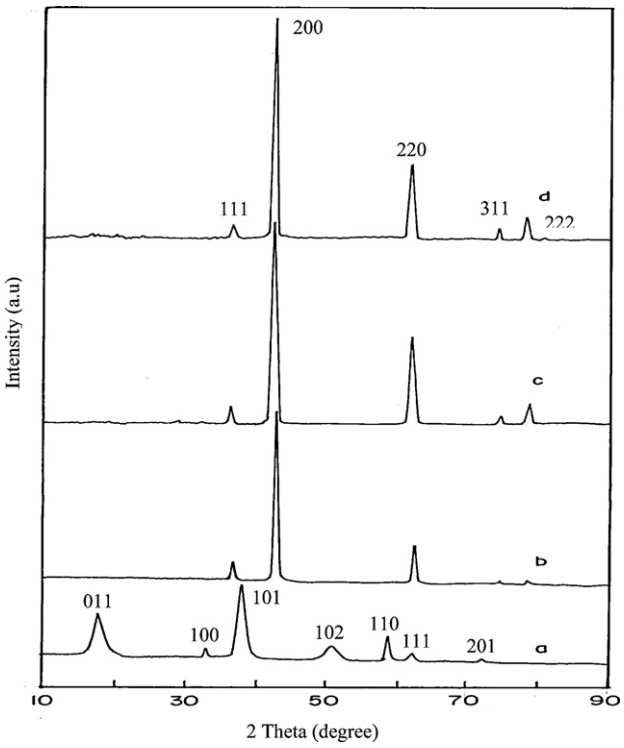

Fig. 1. XRD patterns of the prepared MgO samples: (a) $Mg(OH)_2$ (commercial), (b) MgO bulk (commercial), (c) sample A (microwave method), (d) sample B (conventional method).

The lattice parameters were calculated using the formula given in Eq. (1):

$$\sin^2\theta = \frac{\lambda^2}{4}\left[\frac{4}{3}\left(\frac{h^2+hk+k^2}{a^2}\right)+\frac{l^2}{c^2}\right] \quad (1)$$

where θ is the diffraction angle, λ, the incident wavelength (λ = 0.1540 nm), h, k, and l are Miller's indices. The lattice parameter of sample A is found to be $a = 0.4219$ nm and for sample B is found to be $a = 0.4171$ nm. The average crystallite size was calculated using Scherrer formula [25] given in Eq. (2)

$$L = \frac{0.89\lambda}{\beta\ \cos\theta} \quad (2)$$

where L is the crystallite size, λ, the X-ray wavelength, θ, the Bragg diffraction angle and β, the full width at half maximum (FWHM). The average crystallite size 'L' calculated from the diffraction peaks was found to be around 16–19 nm for sample A and around 78–90 for sample B.

3.2. Fourier transform infrared (FT-IR) analysis

Fourier transform infrared (FT-IR) spectroscopy was used to study the surface interactions of adsorbed water in dynamic

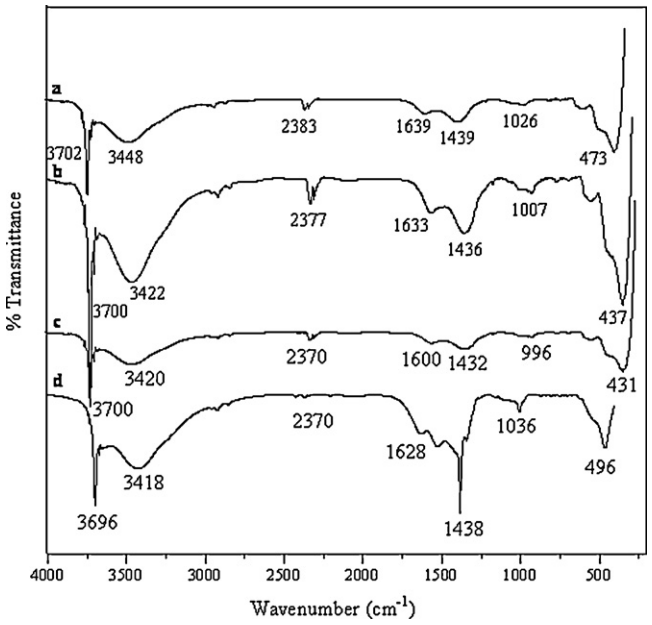

Fig. 2. Fourier transform infrared (FT-IR) spectra of MgO: (a) sample A (microwave method), (b) sample B (conventional method), (c) commercial MgO bulk, (d) commercial $Mg(OH)_2$.

equilibrium with the gas phase on the MgO surface. Frequency shifts and absorbance values were carefully observed to interpret the surface structure of MgO phase. Fig. 2(a, b) shows the FT-IR transmittance spectra of MgO powders produced by microwave assisted combustion method (sample A) and conventional combustion method (sample B) respectively. For the purpose of comparison, we have recorded FT-IR for commercial MgO and $Mg(OH)_2$, which is shown in Fig. 2(c, d). The sharp peak centred at around 3702 cm^{-1} in Fig. 2(a) (sample A) indicates the presence of hydroxyl group on the crystal face of low-coordination sites or defects sites [26]. Since the population of low-coordination sites decreases with increase in crystallite size, the effect is expected to be less pronounced at relatively larger crystallite size. In the present case, crystallite size of sample B are relatively bigger than sample A. So, the absorption is weakened and the peak itself undergoes a red shift of 2 cm^{-1} (3700 cm^{-1}) in spectra (b) is due to the decrease in energy distribution of hydroxyl groups and weak binding of the hydroxyl groups at Mg^{2+} sites in relatively bigger crystallites [7].

It is well-known that H_2O and CO_2 molecules are easily chemisorbed onto MgO surface when exposed to the atmosphere. In spectra (a) and (b), the broad vibration band at 3440–3450 cm^{-1} is associated with the OH stretching vibrations of water molecules, while those at 1630–1640 cm^{-1} are associated with their bending mode. The absorption peak of sample B (spectrum b) undergoes a red shift for H_2O molecule (from 3448 to 3422 cm^{-1} and from 1639 to 1633 cm^{-1}) and becomes weaker when compared with sample A (spectrum a), indicating the reduction in the degree of binding of H_2O on the surface of bigger crystallites due to the reason that they have less atoms/surface unit for the binding interaction with H_2O molecules. In addition, a weak band corresponding to the adsorption of gas-phase CO_2 is visible at around 2375–2385 cm^{-1} and CO_3^{2-} is visible at around 1430–1440 cm^{-1} for both sample A (spectrum a) and B (spectrum b) [27]. However in spectrum (b), the bands are weakened and a red shift is observed for both CO_2 and CO_3^{2-} stretching frequency from 2383 to 2377 cm^{-1} and 1439 to 1436 cm^{-1} respectively, indicating progressive reduction in the degree of binding of CO_2 and CO_3^{2-} molecules at the bigger crystallites. Therefore the bands due to H_2O, CO_2 and CO_3^{2-} groups are unavoidable even at high temperatures. The absorption band noticed around 1026 cm^{-1} (spectrum a) and 1007 cm^{-1} (spectrum b) in the present case is possibly arising due to H^- ion. The strong and broad band at 473 cm^{-1} (spectrum a) and 437 cm^{-1} (spectrum b) are associated with the vibration of Mg–O, which is similar to that reported by Mohandes et al. [28].

3.3. Morphology of MgO micro and nano structures

Fig. 3(a) is a SEM image of aggregated MgO nanosheets (sample A). A magnified SEM image of another zone of the sample in Fig. 3(b) can be seen as nanosheets-like structure. The sheet like morphology with diameter in the range of 3–4 μm and the thickness of a nanosheet in the range of 20–30 nm was observed. Therefore, we can infer that nanosheets have been formed and aggregated during the combustion process in the microwave method. SEM images of MgO micro cubes (sample B) are shown in Fig. 3(c, d), verifying MgO product consisting of a large amount of micro-cubes with nanosheets like structure on the surface. The MgO micro cubes structure is similar to that of the above-mentioned MgO nanosheets in surface phenomena, which further attests that micro cubes structure could be formed in thermal decomposition process and transformed to cubes with nanosheets on the surface when calcinizing at 500 °C for 2 h in the conventional method. The nano sheets structure of sample A is well evident from the HR-SEM images (Fig. 3(a, b)) by the appearance of sharp edges and the flat middle. Although the exact formation mechanism is still under determined, we think that the possible mechanism may be as follows:

The course of the microwave assisted combustion synthesis using a microwave oven operated at a power of 750 W in the present study would have produced enormous amount of heat. This would have resulted in the formation of MgO nano sheets according to the following theoretical reaction of the assumed complete combustion using urea as fuel.

$$2Mg(NO_3)_2{\cdot}6H_2O(s) + 6CO(NH_2)_2(s) + 4O_2(g) \rightarrow 2MgO(s) + 18H_2O(g) + 6CO_2(g) + 8N_2(g)$$

During combustion, the gaseous products released were N_2, CO_2 and H_2O as water vapour. We assume that the brown fumes observed during combustion were released in the form of the above gaseous products. Thus gaseous products can probably form gaseous cavities during the microwave irradiation which can act as heterogeneous nucleation centres for polycrystalline aggregation [29]. The formation of nanosheets can be understood due to the formation of gaseous cavities with release non-uniform gaseous products (N_2, CO_2 and H_2O) [30]. When heating precursor solution by microwave irradiation, the basic magnesium oxide particles form gradually. The particles formed initially are small and dispersed as nuclei, and then more nuclei will aggregate together to form microspheres. When the solution reaches the point of spontaneous combustion, it vaporizes the solution vigorously and becomes a solid where more gaseous products bubble in the inner microsphere. As a result the bubbles will rise producing numerous channels called MgO nanosheets. However in the conventional heating method (at 500 °C with 2 h calcinations in the same temperature) gaseous products which are formed along with MgO micro-cubes will escape making the sheet like structure on the surface and not destroying the micro-cubes structure that is formed. Therefore, it is clearly understood that in the microwave method, the molecular dipoles are induced to oscillate by microwave. This oscillation causes higher rate of molecular collision which generate enormous amounts of heat, consequently the temperature distribution is homogeneous and transferred to the materials interior, making explosion reaction followed by vigorous evolution of gases to form nanosheets structures. But in the conventional heating, there is a temperature gradient between the heat source and the

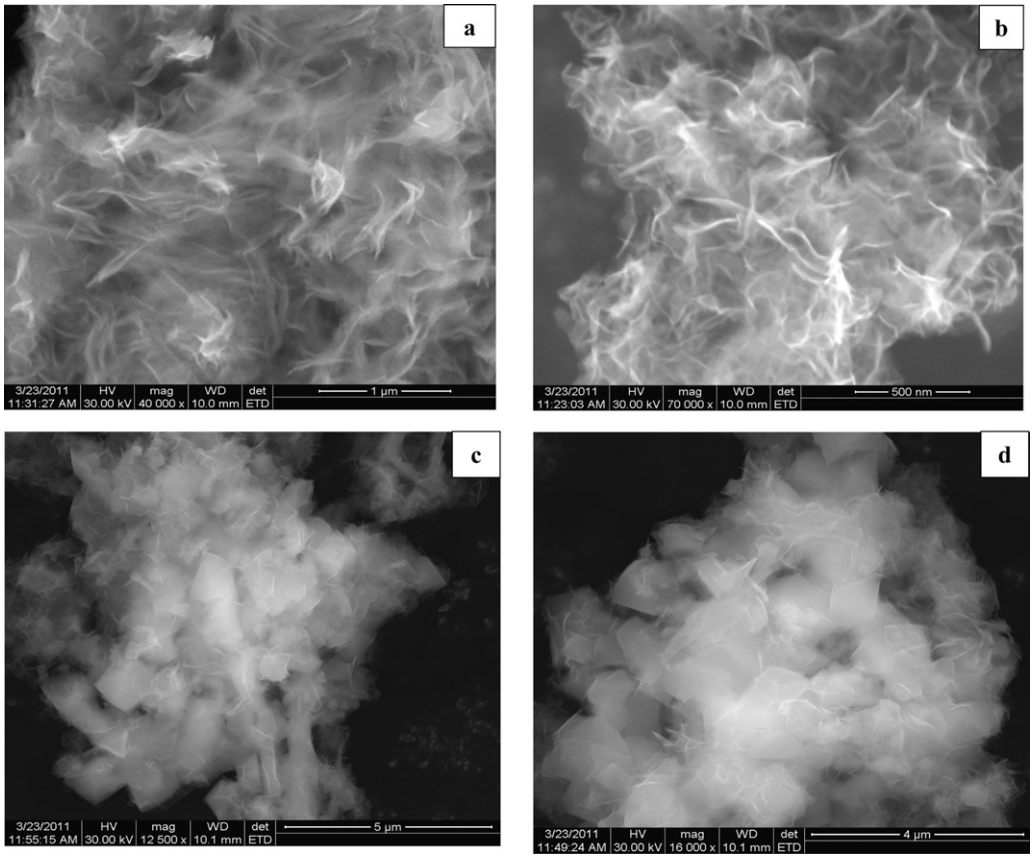

Fig. 3. HR-SEM images of MgO: (a, b) sample A (microwave method), and (c, d) sample B (conventional method).

mass to heat. Thus, during the calcinations process the temperature distribution is not homogeneous and cannot be transferred to the materials interior but spreads more on the surface. Hence the gaseous products on the surface of the MgO material are evolved vigorously and form sheet like structure on the surface [31].

To provide further evidence in the formation of nanosheets from the microspheres of sample A, TEM analysis was carried out only for sample A. A TEM image of typical MgO microsphere is presented in Fig. 4(a), indicating that the nano sheets are agglomerated together. Fig. 4(c, d) are the dark field TEM images of Fig. 4(a, b) respectively, which clearly shows that the nanosheets are made up of nanocrystallites with the size range of 3–7 nm. The particle size distribution histogram is shown in Fig. 4(e). The inset of Fig. 4(a, b) shows corresponding selected area electron diffraction (SAED) pattern. The ring pattern implies that the prepared MgO (sample A) is good crystalline material with polycrystalline nature. Hu et al. [32] reported that nanosheets have potential application in fuel cells and methanol-based alternative energy technologies. In order to have an idea of the absorbance capability of MgO, BET analysis was carried out for sample A and sample B. The surface area and pore volume parameters of MgO are shown in Table 1. Yuna and Guocai [33] reported that nanosheets would be promising candidate material for application in plasma display panels (PDP) or other optical fields. Hence, the as-synthesized MgO nanosheets structures are well known for their luminescent properties which can be utilized in optical fields and has potential application in energy technologies [25]. The composition of obtained MgO was analyzed by means of energy dispersive X-ray analysis (EDX) as shown in Fig. 5(a, b). The EDX result showed the presence of Mg and O by the appearance of Mg and O peaks without any other characteristic peaks. Hence, the results are definitive evidence to suggest that the sample A and B do not contain any other element and are indeed free from other impurities.

Table 1
Surface area and pore volume parameters of MgO.

S. No.	Parameters	Sample code	
		Sample A	Sample B
1	S_{BET} (m^2/g)	63.56	30.70
2	Total pore volume (cm^3/g)	0.317	0.265
3	Average pore diameter (nm)	5.43	3.70

S_{BET} – BET surface area.

3.4. Optical studies (diffused reflectance spectroscopy)

The energy band gap (E_g) of MgO was obtained from the optical diffuse reflectance spectra (DRS) recorded at room temperature and is shown in Fig. 6(a, b). In the UV diffuse reflectance spectrum (b) of sample B, absorption bands at 224 nm (5.53 eV) and 284 nm (4.36 eV) corresponds to the excitation of four-fold and three-fold coordinated O^{2-} anions in edges and corners, respectively. For sample A (spectrum a), the two broad peak positions were considerably blue shifted to 208 (by 16 nm, 5.96 eV) and 280 nm (by 4 nm, 4.42 eV) respectively, due to the size quantization [34]. For pure MgO, the optical excitation of five-fold coordinated O^{2-} anions lies at 185 nm (6.6 eV), i.e., below the wavelength accessible in non-evacuated spectrometers ($\lambda > 200$ nm) [35].

3.5. Photoluminescence (PL) studies

Optical investigations can reveal useful information for understanding the physical properties of materials. It also allows the possibility to extend the potential application of MgO in

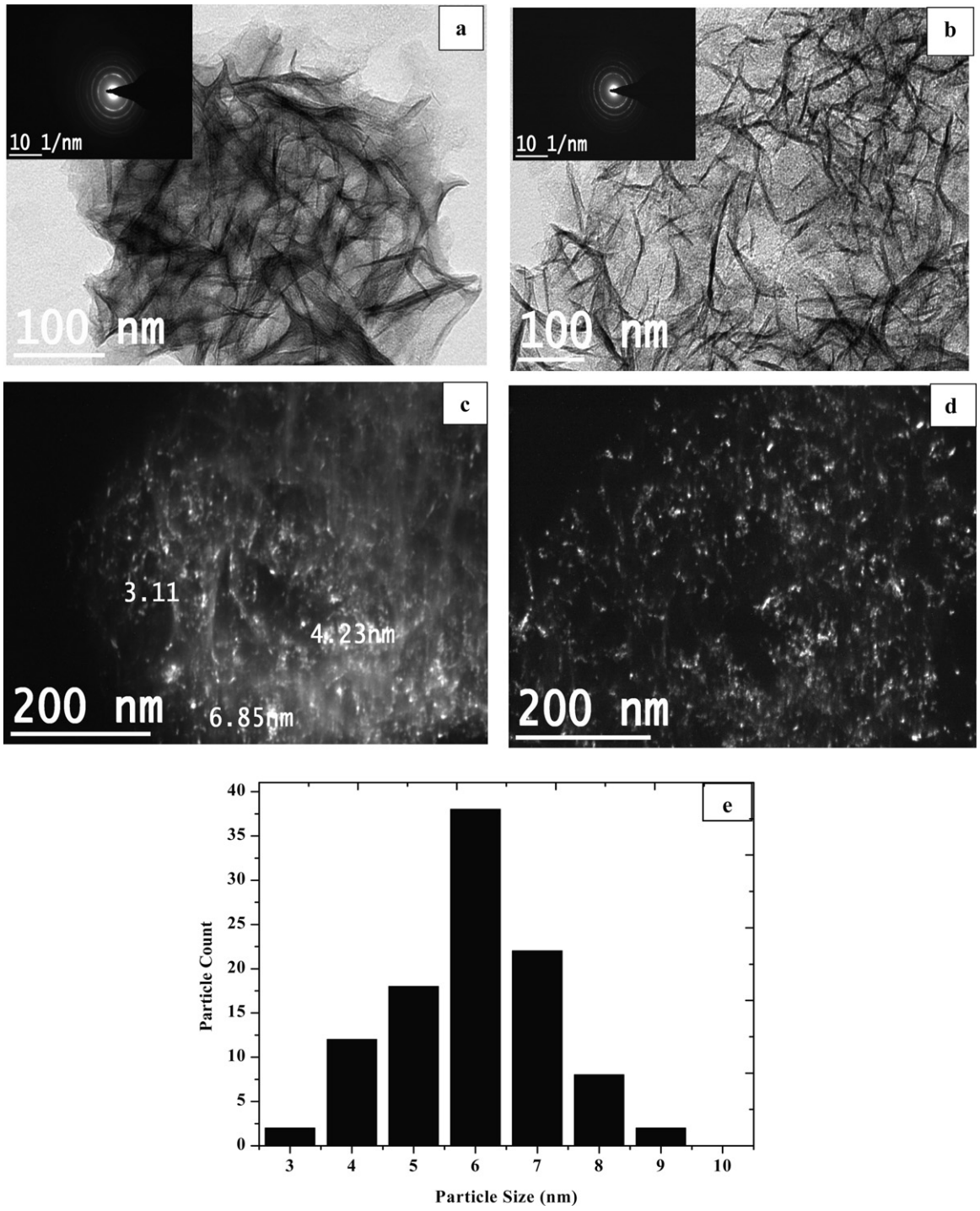

Fig. 4. TEM images of MgO of sample A (microwave method): (a, b) bright field images, (c, d) dark field images and inset of (a, b): corresponding SAED patterns, (e): the particle size distribution histogram.

optoelectronic devices. In our experiments, rapid combustion may generate various structural defects, which generally act as deep defect donors in semiconductor oxide which contribute to the optical emissions. Moreover, the density of defects and surface states may change with formation conditions, morphology and size of the crystallites. It is therefore interesting to examine different defect energy levels. Room temperature PL spectra [Fig. 7(a, b)] of the MgO were measured with an excitation wavelength of 385 nm. Clearly, the PL bands in both spectra (a) and (b) for the sample A and B respectively are not due to the band gap emission, but can be attributed to various structural defects. This would induce the formation of new energy levels in the band gap of MgO. Therefore, in spectrum (b) a broad emission band observed at 437.0 nm (2.83 eV) is arising due to $^3B_{1u} \rightarrow {}^1A_g$ transition of the F_2^{2+} centre in D_{2h} symmetry. This can be compared with the 425–443 nm (2.92–2.80 eV) emission peak reported earlier by Kumar et al. [36]. Moreover, in literature the 390 nm and 530 nm emission bands are present in the PL spectra of bulk MgO with different defect densities [37]. Qin et al. [38] reported the 388 nm and 452 nm bands with various structural defects in MgO. Zhang et al. [39] investigated PL

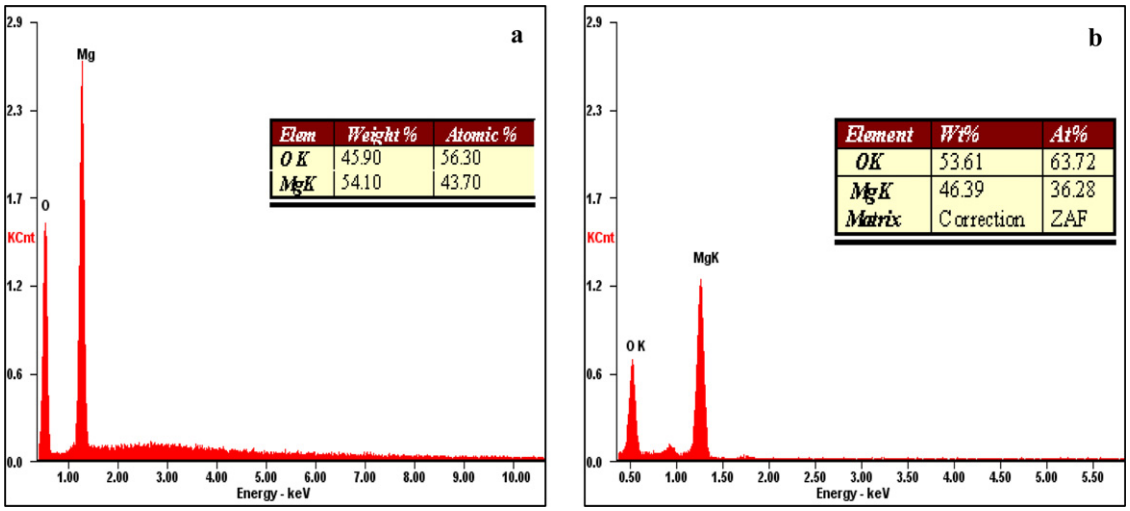

Fig. 5. EDX spectrum of MgO: (a) sample A (microwave method) and (b) sample B (conventional method).

characteristics of MgO nanobelts and found PL bands around 383, 508, and 721 nm as defect state emissions. However, there is a considerable increase in the PL intensity and decrease in the emission wavelength in spectrum (a) (431 nm, 2.87 eV), which shows the low population of H^- ion traps due to reduction in anion vacancy formation. Moreover, the reduced average crystallite size in comparison with sample B may cause this blue shift in emission band due to size effect. There are several additional bands centred at around 465, 490, 530 and 543 nm (in spectrum b) which arise due to energy levels created with various F type anion vacancies. However, these emission bands were considerably blue shifted to 464, 485, 525 and 537 nm respectively with higher PL intensity (in spectrum a) in comparison with spectrum (b). This can be attributed to the increased density of surface defect states because of reduced crystallites size. The blue light emission bands at around 464 (in spectrum a) or 465 (in spectrum b) and 485 (in spectrum a) or 490 nm (in spectrum b) may originate from the recombination of the photogenerated hole with an electron occupying the oxygen vacancy [40]. The green emission bands at around 525 (in spectrum a) or 530 nm (in spectrum b) and 537 (in spectrum a) or 543 nm (in spectrum b) may arise from the emission due to the oxygen ion vacancies (excited F centres) [27]. Thus, if the defect concentration is more, the luminescence intensity also will be more. In general, change in the lattice parameter can be correlated with the concentration of the defects in any undoped material as reported by Janet et al. [27]. The observed increase in the luminescence of sample A (spectrum a) was in good agreement with the lattice parameter value calculated from the XRD data. A decrease or increase from the optimum lattice parameter is an indication of the defect concentration in the respective samples. Hence, it clearly explains the observed higher intense emissions for the sample A, which shows a marked deviation from the optimum lattice parameters. This confirms a good correlation of PL intensity and the lattice parameter. Thus, it is possible to tune the PL intensity of MgO by varying preparation conditions.

It is interesting to investigate the PL spectra of MgO using the excitation wavelength of 290 nm as shown in Fig. 8. The observed broad emission band is centred at around 328, 338, 349, 364, 381, 388 and 398 nm (in spectrum b). However, these emission bands were considerably blue shifted to 314, 337, 347, 360, 375, 384 and 393 nm respectively with higher PL intensity (in spectrum a) in comparison with spectrum (b) due to reduced crystallite size. These observed PL band is not the band gap emission, but can be attributed to various structural defects. Selvamani et al. [41] investigated the PL characteristics of MgO micro-sheets and found the broad emission band with peaks centred at 354, 384 and 400 nm. For other MgO nanostructures, Kumari et al. [42] reported the PL peaks centred at around 354, 382, 415 and 465 nm due to

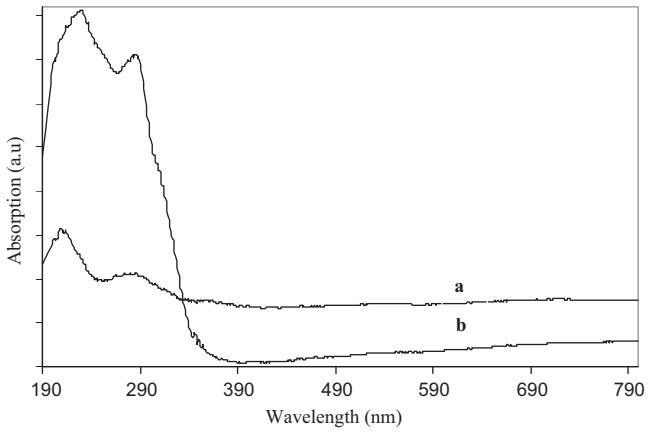

Fig. 6. Diffuse reflectance spectra (DRS) of the prepared MgO: (a) sample A (microwave method), (b) sample B (conventional method).

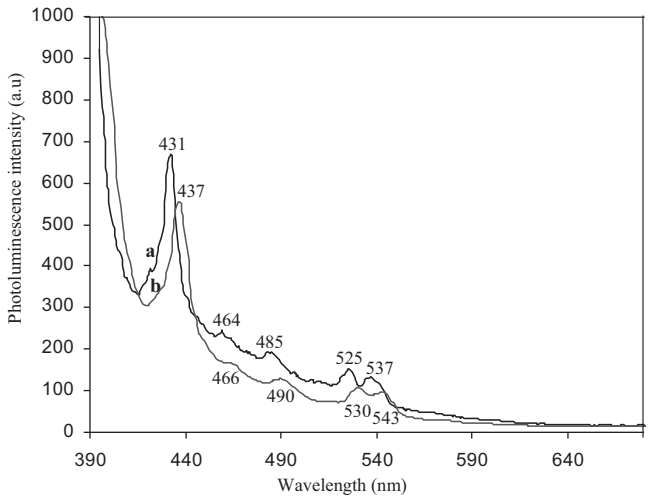

Fig. 7. Room temperature PL spectra of MgO (excited at 385 nm): (a) sample A (microwave method), (b) sample B (conventional method).

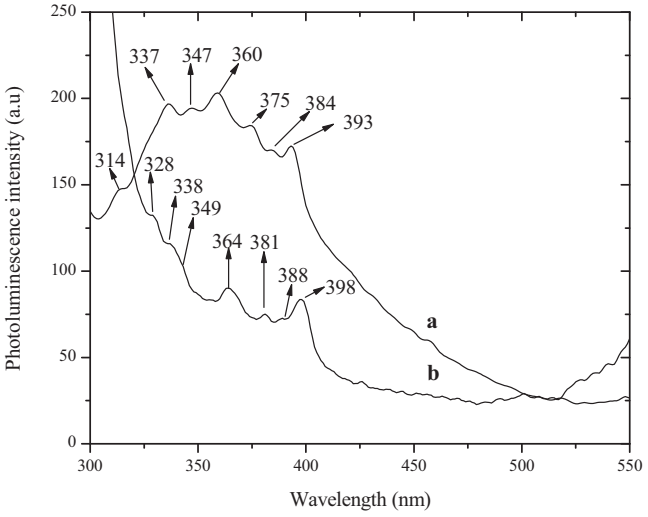

Fig. 8. Room temperature PL spectra of MgO (excited at 292 nm): (a) sample A (microwave method), (b) sample B (conventional method).

the oxygen ion vacancy. Therefore in our case, various structural defects, such as oxygen vacancy act as deep defect donors and would induce the formation of new energy levels in the band gap of MgO.

4. Conclusions

MgO nanostructures have been successfully synthesized by a simple and rapid microwave-assisted combustion method and MgO micro-structures by conventional combustion method using urea as the fuel. In comparison with conventional heating, microwave-assisted combustion method shortens the reaction time. The heating is not only quick but also uniformly spread through the entire bulk of the reaction mixture. This may result in the formation of nano sheets structure with narrow distribution of particle size. A plausible mechanism has been proposed for the formation of nanosheets. A clear correlation was made with PL intensity and the lattice parameter of the MgO, which will open up the possibilities for predicting the optical properties by looking into the XRD data. The photoluminescent MgO micro and nano-structures may have potential application on the design of safe, inexpensive and environmentally benign optical materials. Thereby, it is confirmed that the synthesized MgO (sample A and B) showed good optoelectronic properties. Therefore, our methodology and experiments may promote the control of desired morphologies of other functional oxide materials. Moreover, the microwave-assisted combustion method is an economical and rapid method for the preparation of MgO nanostructures when compared to the conventional method with respect to energy, time and simplicity.

Acknowledgements

The authors duly acknowledge the financial support rendered by the Department of Science and Technology (DST), New Delhi, India (Project number: DST (Ref. No. SR/FTP/CS-117/2007)).

References

[1] G. Zhang, H. Hattori, K. Tanabe, Appl. Catal. 36 (1988) 189.
[2] M.J. Baird, J.H. Lunsford, J. Catal. 26 (1972) 440.
[3] J. Schwank, S. Galvagno, G. Parravano, J. Catal. 63 (1980) 415.
[4] G.W. Wagner, P.W. Bartram, O. Kopper, K.J. Klabunde, J. Phys. Chem. B 03 (1999) 3225.
[5] R.Z. Ma, Y. Bando, Chem. Phys. Lett. 370 (2003) 770.
[6] Y.S. Yuan, M.S. Wong, S.S. Wang, J. Mater. Res. 11 (1996) 8.
[7] A. Kumar, J. Kumar, J. Phys. Chem. Solids 69 (2008) 2764.
[8] H. Fang, B. Hu, L. Wang, R. Lu, C. Yang, Front. Chem. China 3 (2008) 193.
[9] Y. Ding, G. Zhang, H. Wu, B. Hai, L. Wang, Y. Qian, Chem. Mater. 13 (2001) 435.
[10] H. Niu, Q. Yang, K. Tang, Y. Xie, J. Nanopart. Res. 8 (2006) 881.
[11] M.E. Shall, W. Slack, W. Vann, D. Kane, D. Hanley, J. Phys. Chem. 98 (1998) 3067.
[12] J.S. Matthews, O. Just, B.O. Johnson, W.S. Rees, J. Chem. Vapor Deposition 6 (2000) 129.
[13] A. Bhargava, J. Alarco, I. Mackinnon, D. Page, A. Ilyushechkin, Mater. Lett. 34 (1998) 133.
[14] F. Khairallah, A. Glisenti, J. Mol. Catal. Chem. 274 (2007) 137.
[15] A. Subramania, G.V. Kumar, A.R.S. Priya, T. Vasudevan, Nanotechnology 18 (2007) 225601.
[16] K. Aslan, C.D. Geddes, Plasmonics 3 (2008) 89.
[17] M. Nuchter, B. Ondruschka, W. Bonrath, A. Gum, Green Chem. 6 (2004) 128.
[18] C. Gabriel, S. Gabriel, E.H. Grant, B.S.J. Halstead, D.M.P. Mingos, Chem. Soc. Rev. 27 (1998) 213.
[19] R.V. Mangalaraja, J. Mouzon, P. Hedstrom, C.P. Camurri, S. Ananthakumar, M. Oden, Powder Technol. 191 (2009) 309.
[20] H. Mohebbi, T. Ebadzadeh, F.A. Hesari, Powder Technol. 188 (2009) 183.
[21] I. Ganesh, R. Johnson, G.V.N. Rao, Y.R. Mahajan, S.S. Madavendra, B.M. Reddy, Ceram. Int. 31 (2005) 67.
[22] Y.C. Hong, H.S. Uhm, Chem. Phys. Lett. 422 (2006) 174.
[23] S. Baskoutas, P. Giabouranis, S.N. Yannopoulos, V. Dracopoulos, L. Toth, A. Chrissanthopoulos, N. Bouropoulos, Thin Solid Films 515 (2007) 8461.
[24] O. Coovattanachai, N. Tosangthum, M. Morakotjinda, T. Yotkaew, R. Krataitong, B. Vetayanugul, R. Tongsri, Songklanakarin, J. Sci. Technol. 32 (2010) 163.
[25] R. Bouberki, Z. Beji, K. Elkabous, F. Herbst, G. Viau, S. Ammar, F. Fievet, J.H.V. Bardeleben, A. Mauger, Chem. Mater. 21 (2009) 843.
[26] M. Foster, M. Furse, D. Passno, Surf. Sci. 502 (2002) 102.
[27] C.M. Janet, B. Viswanathan, R.P. Viswanath, T.K. Varadarajan, J. Phys. Chem. C 111 (2007) 10267.
[28] F. Mohandes, F. Davar, M.S. Niasari, J. Phys. Chem. Solids 71 (2010) 1623.
[29] Y.C. Zhanga, G.L. Wanga, X.Y. Hua, W.D. Zhou, J. Cryst. Growth 285 (2005) 600.
[30] Y.J. He, Mater. Lett. 60 (2006) 3511.
[31] E. Esmaeili, A. Khodadadi, Y. Mortazavi, J. Eur. Ceram. Soc. 29 (2009) 1061.
[32] J. Hu, K. Zhu, L. Chen, C. Kubel, R. Richards, J. Phys. Chem. C 111 (2007) 12038.
[33] Z. Yuna, Z. Guocai, Mater. Sci. Eng. B 142 (2007) 93.
[34] S. Stankic, M. Muller, O. Diwald, M. Sterrer, E.J. Bernardi, Angew. Chem. Int. Ed. 44 (2005) 4917.
[35] F. Gu, C. Li, H. Cao, W. Shao, Y. Hu, J. Chen, A. Chen, J. Alloys Compd. 453 (2008) 361.
[36] A. Kumar, S. Thota, S. Varma, J. Kumar, J. Luminescence 131 (2011) 640.
[37] G.H. Rosenblatt, M.W. Rowe, G.P. Williams Jr., R.T. Williams, Y. Chen, Phys. Rev. B 39 (1989) 10309.
[38] L. Qin, J. Zhao, X. Zou, Mater. Chem. Phys. 113 (2009) 468.
[39] J. Zhang, L. Zhang, Chem. Phys. Lett. 363 (2002) 293.
[40] Y. Hao, G. Meng, C. Ye, X. Zhang, L. Zhang, J. Phys. Chem. 109 (2005) 11204.
[41] T. Selvamani, A. Sinhamahapatra, D. Bhattacharjya, I. Mukhopadhyay, Mater. Chem. Phys. 129 (2011) 853.
[42] L. Kumari, W.Z. Li, C.H. Vannoy, R.M. Leblanc, D.Z. Wang, Ceram. Int. 35 (2009) 3355.